photonics

MDPI

Article

Characteristics of Ultrasensitive Hexagonal-Cored Photonic Crystal Fiber for Hazardous Chemical Sensing

Abdul Mu'iz Maidi [1,*], Norazanita Shamsuddin [1], Wei-Ru Wong [2], Shubi Kaijage [3] and Feroza Begum [1]

[1] Faculty of Integrated Technologies, Universiti Brunei Darussalam, Jalan Tungku Link, Gadong, Bandar Seri Begawan BE1410, Brunei; norazanita.shamsudin@ubd.edu.bn (N.S.); feroza.begum@ubd.edu.bn (F.B.)
[2] Department of Electrical Engineering, Faculty of Electrical Engineering, Universiti Malaya, Kuala Lumpur 50603, Malaysia; weiru@um.edu.my
[3] School of Computational and Communication Science and Engineering, Nelson Mandela African Institution of Science and Technology, Arusha 23311, Tanzania; shubi.kaijage@nm-aist.ac.tz
* Correspondence: 17b4010@ubd.edu.bn

Abstract: A highly sensitive non-complex cored photonic crystal fiber sensor for hazardous chemical sensing with water, ethanol, and benzene analytes has been proposed and is numerically analyzed using a full-vector finite element method. The proposed fiber consists of a hexagonal core hole and two cladding air hole rings, operating in the lower operating wavelength of 0.8 to 2.6 µm. It has been shown that the structure has high relative sensitivity of 94.47% for water, 96.32% for ethanol and 99.63% for benzene, and low confinement losses of 7.31×10^{-9} dB/m for water, 3.70×10^{-10} dB/m ethanol and 1.76×10^{-13} dB/m benzene. It also displays a high power fraction and almost flattened chromatic dispersion. The results demonstrate the applicability of the proposed fiber design for chemical sensing applications.

Keywords: photonic crystal fiber; chemical sensor; relative sensitivity; confinement loss

Citation: Maidi, A.M.; Shamsuddin, N.; Wong, W.-R.; Kaijage, S.; Begum, F. Characteristics of Ultrasensitive Hexagonal-Cored Photonic Crystal Fiber for Hazardous Chemical Sensing. *Photonics* **2022**, *9*, 38. https://doi.org/10.3390/photonics9010038

Received: 10 December 2021
Accepted: 3 January 2022
Published: 10 January 2022

1. Introduction

In both industry and academic sectors, photonic crystal fibers (PCFs) are one of the most interested research areas in the field of fiber optics. The huge popularity of PCF arises from its characteristics of low loss in optical signal, more flexibility and lower weight [1]. These benefits mean that various materials can be incorporated to form the structure of the PCF to promote a photonic band gap and modified total internal reflection (m-TIR) propagation mode due to the high refractive index difference. It, additionally, is not restrained to communication applications but also can be effectively employed in different promising applications, such as astronomy, security and imaging [2,3]. Moreover, PCF can be used in diverse chemical and biological sensing applications such as temperature [4], pressure [5], mechanical [6], gas [7] and liquid [8] sensors. PCF can be employed as a sensor by incorporating the core air holes with different test analytes; thus, it is applicable in various sectors. One of the most popular operations of PCF in the field of sensing includes its use as a chemical sensor, where a group of pioneering researchers have introduced diverse designs with varying performance over the years.

A group of researchers [9] introduced a sensor design composed of three layers of cladding air holes in a circular lattice with an array of elliptical holes as the core for chemical sensing, with ethanol as the test analyte. The relative sensitivity was 29.25% and confinement loss was in the order of 10^{-7} dB/m, acquired at 1.5 µm operating wavelength. In reference [10], a hexagonal grid PCF sensor, with four cladding air hole rings and a single core elliptical hole, for liquid detection with a water analyte, has been proposed. It shows values of λ = 1.3 µm, low relative sensitivity of 41.37% and an order of 10^{-10} dB/m for confinement loss. Bin Murshed Leon et al. [11] also proposed a PCF design with water

as the test analyte. The design of the PCF structure consists of four rings of cladding air holes in a hexagonal arrangement and an array of nine circular holes designated as the core. Such a sensor design allowed a relative sensitivity of 44.45% and confinement loss of approximately 10^{-7} dB/m at a 1.3 μm operating wavelength. The same research group [12] also introduced a design with four cladding air hole rings and four circular holes arranged as the core of the fiber, with a similar liquid analyte: water. At an optimum wavelength of 1.3 μm, it results in a low relative sensitivity of 49.13% and confinement loss of order 10^{-5} dB/m. Islam et al. [13] suggested a chemical analyte sensor with water, ethanol and benzene, which yielded relative sensitivity results of 48.19%, 53.22% and 55.56% for water, ethanol and benzene, respectively, achieved at a wavelength of 1.3 μm. Then, reference [14] reported relative sensitivities of 56.75% for water, 52.07% for ethanol and 58.86% for benzene and a confinement loss of approximately 10^{-5} dB/m for all the test analytes, at λ = 1.33 μm, with five ring cladding holes in an octagonal lattice and nine core holes in a square configuration, proposed as the PCF chemical sensor. A PCF structure with three cladding air hole rings has also been proposed by Maidi et al. [15]. In contrast to the comparatively simple chemical sensor with water, ethanol and benzene marked on the three elliptical core holes, the PCF exhibits decent results, with relative sensitivities of 62.60%, 65.34% and 74.50% for water, ethanol and benzene, respectively, with confinement losses in the order of 10^{-7} dB/m, 10^{-8} dB/m and 10^{-11} dB/m for water, ethanol and benzene, respectively, at λ = 1.3 μm. Notably, a group of researchers [16] recommended an impressively performing PCF structure of one hexagonal core and five cladding rings in a circular form for chemical sensing, demonstrating high relative sensitivities. Relative sensitivities of 88.93%, 91.87% and 97.89% were achieved for water, ethanol and benzene, respectively, and the confinement losses for the PCF were in the order of approximately 10^{-10} dB/m for all test analytes. These values were obtained at an optimum wavelength of 1.55 μm. In the literature [9–16], researchers focused on implementing elaborative PCF structures, which consist of intricate core designs and multiple layers of cladding holes to produce good outcomes in the simulated optical parameters. With such expressive designs, this increases the difficulty of manufacturing the PCFs and may affect the sensing results due to the fabrication tolerances. Fabrication of PCFs is subject to manufacturing errors and prone to issues such as inaccuracy of hole sizes due to the irregular shape and positioning of the desired holes [17,18]. Furthermore, a single inaccuracy in an air hole will affect surrounding air holes as well, which can be problematic in elaborate designs with intricate fiber core structures and numerous air holes [19].

In this work, a noncomplex PCF structure is proposed that maintain impressive results of optical properties, particularly its relative sensitivity and confinement loss. Results of the effective refractive index, relative sensitivity, power fraction, confinement loss and chromatic dispersion are investigated, as well, over the infrared region from 0.8 to 2.6 μm operating wavelength. Water, ethanol and benzene are selected as the test analytes for the study.

2. Design

The sensing principles for PCF sensors are based on the interaction between the optical signal and the analyte in the propagation core region [20]. The evanescent field of light is imposed on the PCF and extends to the located analyte to be sensed. The presence of cladding air holes allows near-total confinement of light to promote sufficient light–analyte interaction. Thus, an appropriate geometry of the proposed PCF sensor was configured and is presented in Figure 1, which consists of a core, cladding and the perfectly matched layer (PML). Silica was chosen for the background material established for the cladding and PML, marked in red and blue colors, respectively. Likewise, the white color indicates air for the cladding air holes and the test analytes are shown in yellow at the core.

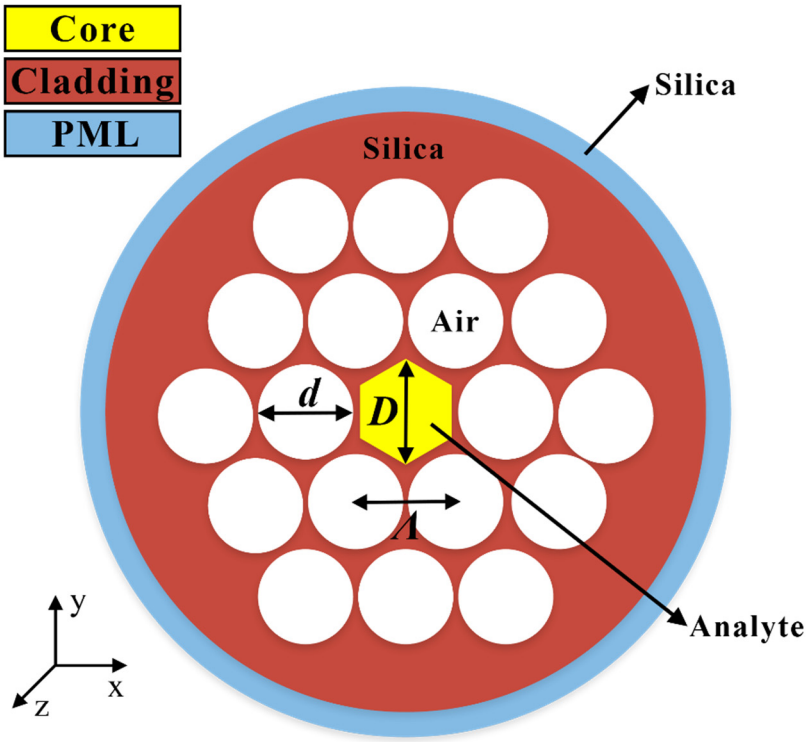

Figure 1. Schematic of the design proposed for the PCF.

The core of the fiber is a hollow hexagonal hole, where the selective test analyte is suggested to be administered for chemical sensing. The corner-to-corner length of the hexagonal hole is denoted as l. The cladding consists of multiple air holes positioned throughout its region, and each circular air hole is denoted as d. To offer a symmetrical design, the cladding holes are situated equidistantly from each other, with a pitch distance denoted as Λ = 3.0 µm and air-filling fraction (AFF) of 0.97. The cladding has a total of 18 air holes arranged in 2 rings. The PML is imposed on the fiber structure to absorb light leaked from the core and cladding region. The dimension of the core l = 3.32 µm, and the diameter of each cladding air hole d = 2.91 µm. The PML is enhanced to be 10% of the fiber diameter to meet the boundary condition. The proposed PCF sensor can detect various chemical analytes; however, the selected test analytes in this paper are water, ethanol and benzene. The air-filling fraction of the cladding is kept at a high value to acquire an optically dense core compared to the cladding, which preserves the modified total internal reflection (m-TIR) as the guiding mechanism.

There are various possible fabrication methods that have been introduced, such as the sol–gel technique [21], stacking [22], drilling [23], 3D printing [24] and extrusion [25]. The fabrication of this PCF sensor design can be performed using the extrusion method as it allows the fabrication of intricate designs with high accuracy. Additionally, the infiltration of the test chemical analyte into the hollow holes can be achieved by using the selective infiltration technique, which has been experimentally introduced by researchers [26–30]. This technique is capable of injecting liquids into the micro-structured core and cladding holes in the PCF. Numerous methods for injecting liquid analytes have been proposed by researchers throughout the years, including the multi-step injection-cure-cleave process [26], fusion splicer [27], lateral filling [28], femtosecond laser micromachining [29] and focused ion beam micromachining [30].

3. Methodology

A simulation of the proposed PCF has been conducted applying the full-vector finite element method (FV-FEM) for numerical analysis using COMSOL Multiphysics software version 5.5. A finer meshing type has been selected for the design to be correctly mapped.

The complete mesh consists of 14,370 triangular elements, 1352 edge elements and 86 vertex elements. The proposed PCF is intended for detecting chemicals, particularly water, ethanol and benzene. Figure 2 shows the refractive index of silica and the test analytes (water, ethanol and benzene) with respect to a micrometer wavelength of 0.8–2.6 µm [31–34].

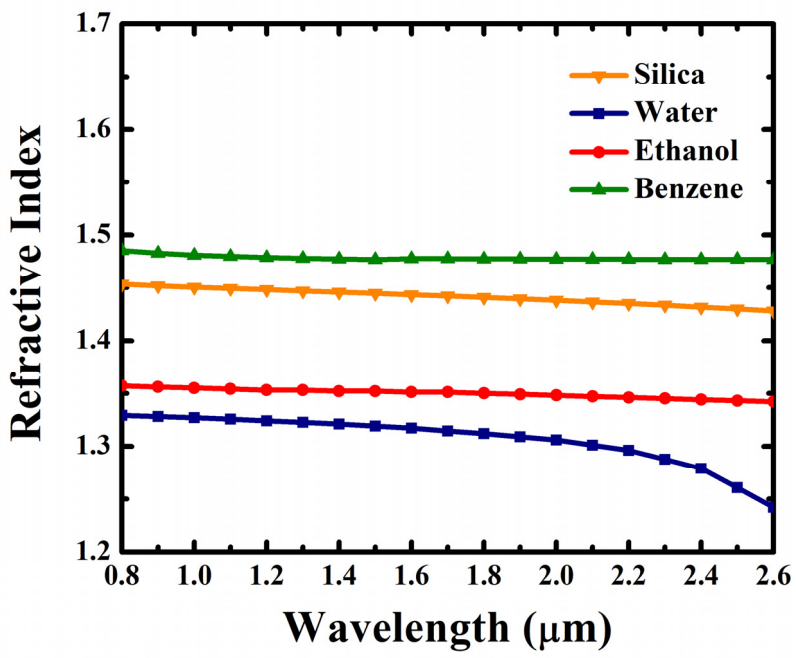

Figure 2. Refractive index of silica and test analytes, water, ethanol and benzene, at 0.8–2.6 µm operating wavelength [31–34].

Evaluation of the performance and practicability of the proposed PCF design is conducted through investigating the respective optical properties: effective refractive index, relative sensitivity, power fraction, confinement loss and chromatic dispersion.

With silica as the background material, hollow air holes and core holes that have been set with the test analytes, the effective refractive index n_{eff} can be quantified and modeled using Sellmeier's equation given by [35]:

$$n_{\text{eff}}(\lambda) = \sqrt{1 + \frac{B_1\lambda^2}{\lambda^2 - C_1} + \frac{B_2\lambda^2}{\lambda^2 - C_2} + \frac{B_3\lambda^2}{\lambda^2 - C_3}} \quad (1)$$

where λ is the operating wavelength and B_i and C_i (i = 1,2 and 3) are the Sellmeier coefficients for the specific material.

Relative sensitivity S determines the practicability of the PCF sensor to detect analytes by matching the refractive indices and achieved by measuring the light intensity that interacts with the analyte to be detected. It is defined as [15,36,37]:

$$S = \frac{n_{\text{r}}}{n_{\text{eff}}} \times P \quad (2)$$

where n_r is the refractive index of the sensed material and P is the power fraction. The variation in relative sensitivity is closely related to the effective refractive index and power fraction.

Power fraction P is a measure of the amount of power flowing through the PCF at a specific region, and it is defined as the ratio of power in a chemical-filled region to that of the total fiber by integration. It is expressed by Poynting's theorem as [15,36,37]:

$$P = \frac{(sample)\int Re(E_xH_y - E_yH_x)dxdy}{(total)\int Re(E_xH_y - E_yH_x)dxdy} \times 100 \quad (3)$$

where E_x, E_y and H_x, H_y are the transverse electric and magnetic fields of the guided mode, respectively. The integral in the numerator is selected over the analyte at the core, whilst the integral in the denominator is over all fiber regions.

Confinement loss L_c describes the phenomenon of leakage of light from the core to the cladding, contributed by the structural design of the fiber. It quantifies the portion of light loss from the core area to the cladding, and is defined as [38–40]:

$$L_c = \frac{40\pi}{\ln(10)\lambda} \mathrm{Im}[n_{\mathrm{eff}}] \times 10^6 \quad (4)$$

where $\mathrm{Im}[n_{\mathrm{eff}}]$ is the imaginary part of the effective mode index. The variations in the operating wavelength and effective refractive index determine the confinement loss.

Chromatic dispersion D is a measure of the light-guiding capabilities of the fiber and the degradation of the mode in the fiber. It is defined as [10,38,40]:

$$D = -\frac{\lambda}{c}\frac{d^2}{d\lambda^2} Re[n_{\mathrm{eff}}] \quad (5)$$

where c is the speed of light and $Re[n_{\mathrm{eff}}]$ is the real part of the effective refractive index.

4. Results and Discussion

Figure 3 illustrates the mode profiles for the different chemical-infiltrated analytes in the core, with an operating wavelength of 1.3 µm. The interaction of light occurs through the core region, with the mode field completely confined at the core for all three test analytes: water, ethanol and benzene.

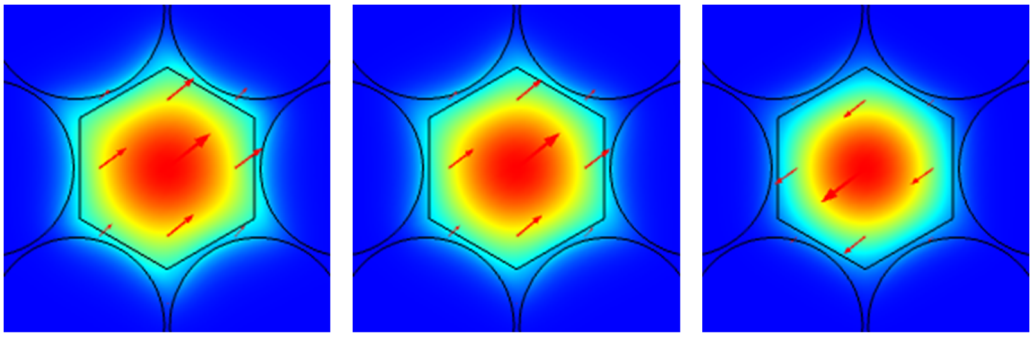

(**a**) (**b**) (**c**)

Figure 3. Mode profile of the proposed PCF for (**a**) water, (**b**) ethanol and (**c**) benzene.

Theoretically, the effective refractive index decreases with an increase in the operating wavelength, and a similar trend is established as well for the proposed PCF shown in Figure 4, with the effective refractive index declining as the operating wavelength is increased, for all the selected analytes: water, ethanol and benzene. This behavior arises where smaller electromagnetic wavelengths propagate through the high refractive index region. Moreover, it can be observed that the effective refractive index of water is the lowest, followed by ethanol and benzene, being the highest, as established from their respective refractive indices, as seen in Figure 2.

It can be seen from Figure 5 that the relative sensitivity for benzene decreases over the scale of set wavelengths from 0.8 to 2.6 µm; however, the trend for water and ethanol increases from 0.8 to 1.3 µm and then subsequently decreases as the wavelength is increased further. Relative sensitivity is closely related to the effective refractive index and power fraction; hence, benzene has the highest relative sensitivity, followed by ethanol and water. At the operating wavelength of 1.3 µm, relative sensitivities are 94.47%, 96.32% and 99.63% for water, ethanol and benzene, respectively. Since the operating wavelength of 1.3 µm yielded the optimum relative sensitivities for water and ethanol, other optical properties

for the proposed PCF were considered at this optimum wavelength. Moreover, as seen from Figure 1, the dimension of the core hole is larger than the surrounding air holes in the cladding, which allows more test analyte to be injected into the core hole; this leads to a stronger interaction between light and the test analyte. Hence, the PCF leads to higher relative sensitivity.

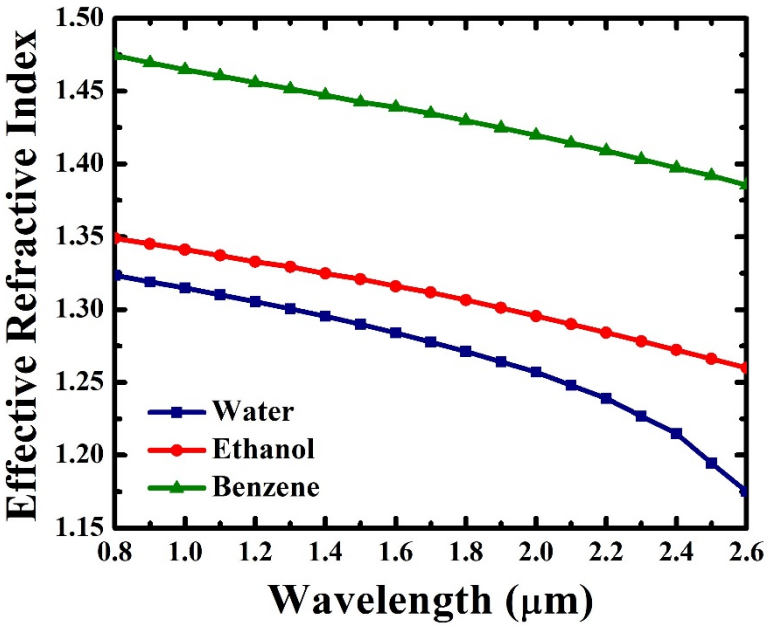

Figure 4. Effective refractive index of the proposed design against operating wavelength for water, ethanol and benzene.

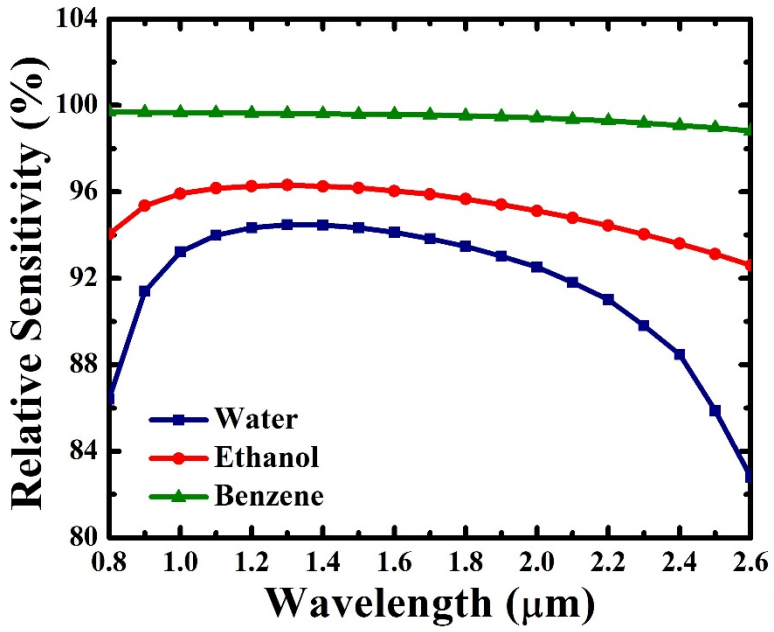

Figure 5. Proposed PCF sensor results for relative sensitivity with respect to wavelength for water, ethanol and benzene.

Figure 6 shows the power fraction of the proposed PCF sensor against different operating wavelengths for water, ethanol and benzene. The amount of power flowing through at the core of the PCF is quantified with this property. It can be seen that the power fractions for water and ethanol present an increasing behavior initially as the operating

wavelength increases between 0.8 and 1.3 µm, before drastically decreasing with further increases in the operating wavelength, whereas the power fraction trend for benzene decreases as the wavelength increases. The decreasing behavior results in optical power leaks from the core region to the surrounding cladding as the wavelength increases. The proposed PCF yields power fractions of 92.91%, 94.64% and 97.84% for water, ethanol and benzene, respectively, at a wavelength of 1.3 µm.

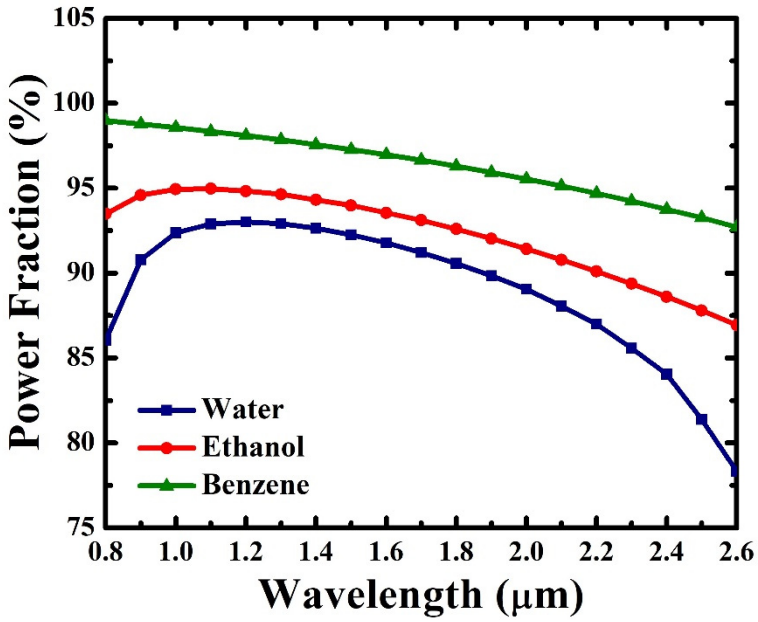

Figure 6. Power fraction of the PCF sensor with respect to wavelength for water, ethanol and benzene.

Figure 7 demonstrates the relationship between confinement loss and operating wavelength. Confinement loss is a measure of light leakage from the core to the cladding, and, in theory, confinement losses generally increase as light tends to leak out of the cladding with respect to the increase in operating wavelength; this characteristic can be seen in the figure. Confinement losses are 7.31×10^{-9} dB/m for water, 3.70×10^{-10} dB/m for ethanol and 1.76×10^{-13} dB/m for benzene, at an operating wavelength of 1.3 µm. Furthermore, with the benefit of a definite hexagonal core and surrounding air hole configuration, it influences the careful confinement of light, as seen in the results.

Figure 8 shows the relationship between the chromatic dispersion of the proposed PCF and the operating wavelength with water, ethanol and benzene. It can be observed that the obtained dispersion is especially low and nearly flattened for all test analytes. This indicates a good result in the interaction between the light signal and the chemical analytes. At a 1.3 µm wavelength, the chromatic dispersions are -0.0053 ps/nm.km for water, -0.0049 ps/nm.km for ethanol and -0.0045 ps/nm.km for benzene. This evaluation of chromatic dispersions is achieved due to the narrow width of the waveguide.

Additionally, regarding the fabrication of the proposed PCF sensor, a tolerance analysis is performed by varying the global parameters—the pitch and diameter of the holes—and examining the effects on the variations in the optical properties: relative sensitivity and confinement loss. Analyses in the order of $\pm 1\%$, $\pm 2\%$ and $\pm 4\%$ are applied on the parameters of the proposed PCF, which is shown in Table 1. A very small effect is seen on the optical properties. In terms of the values of relative sensitivities and confinement losses, they decrease as the percentage variations are increased and they increase when the variations are decreased.

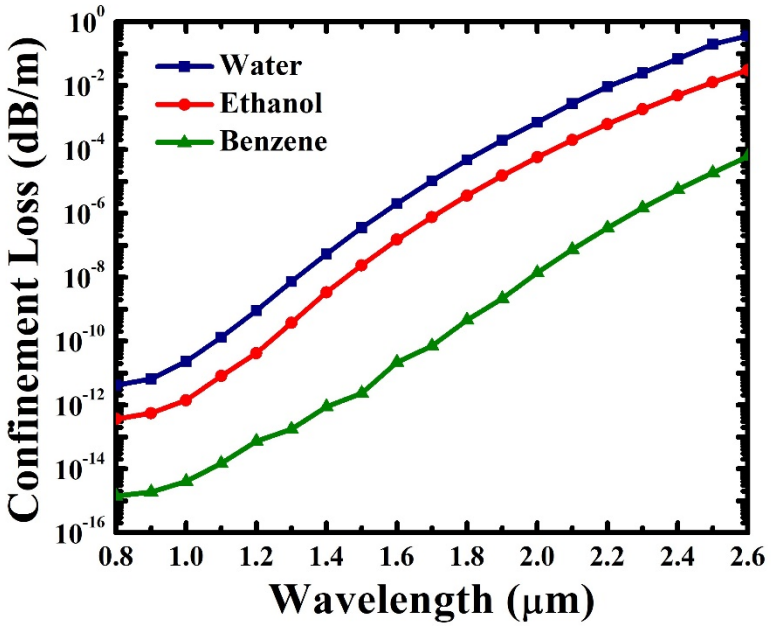

Figure 7. Confinement loss of the PCF sensor with respect to wavelength for water, ethanol and benzene.

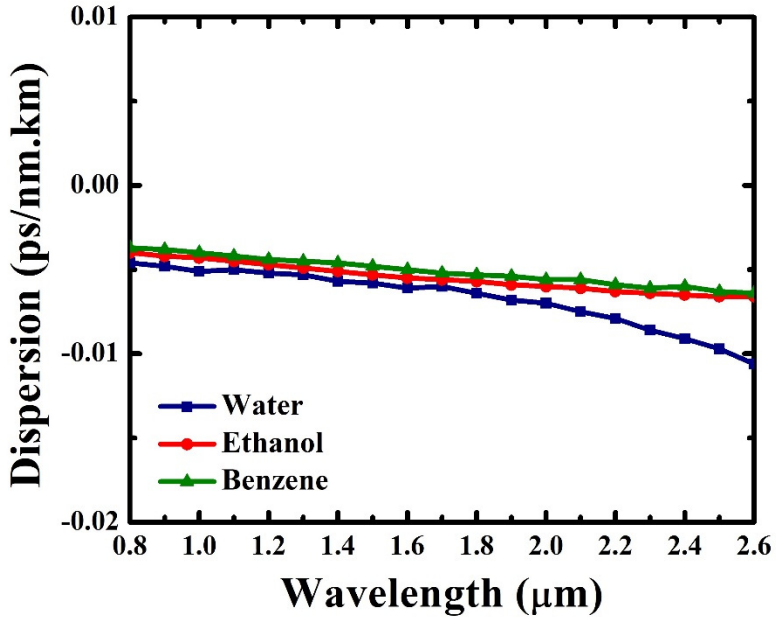

Figure 8. Chromatic dispersion of the proposed design with respect to wavelength for water, ethanol and benzene.

Table 1. Comparison among the variation in global parameters on optimum parameters at λ = 1.3 μm.

Change in Global Parameters	Relative Sensitivity (%)			Confinement Loss (dB/m)		
	Water	Ethanol	Benzene	Water	Ethanol	Benzene
+4%	94.40	96.32	99.64	2.60×10^{-9}	1.05×10^{-10}	7.62×10^{-14}
+2%	94.44	96.32	99.63	4.37×10^{-9}	1.78×10^{-10}	1.28×10^{-13}
+1%	94.46	96.32	99.63	5.58×10^{-9}	2.71×10^{-10}	1.72×10^{-13}
Optimum	94.47	96.32	99.63	7.31×10^{-9}	3.70×10^{-10}	1.76×10^{-13}
−1%	94.49	96.31	99.63	9.54×10^{-9}	4.62×10^{-10}	4.82×10^{-13}
−2%	94.50	96.31	99.62	1.25×10^{-8}	6.78×10^{-10}	5.46×10^{-13}
−4%	94.51	96.30	99.62	2.16×10^{-8}	1.25×10^{-9}	6.71×10^{-13}

Figure 9a–c show the relative sensitivity variations of order ±1%, ±2% and ±4% for water, ethanol and benzene, respectively. Meanwhile, Figure 10a–c illustrate the variations in confinement loss in the order of ±1%, ±2% and ±4% for water, ethanol and benzene, respectively. With such modification made to the dimensions of the pitch and air holes' diameter, Figures 9 and 10 demonstrate minute alterations in the results of the optical properties.

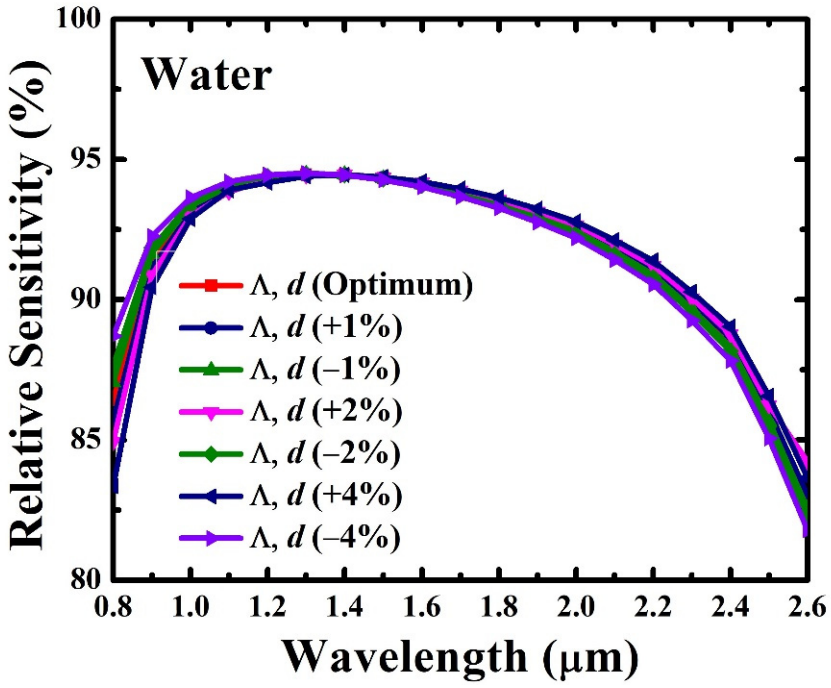

(**a**)

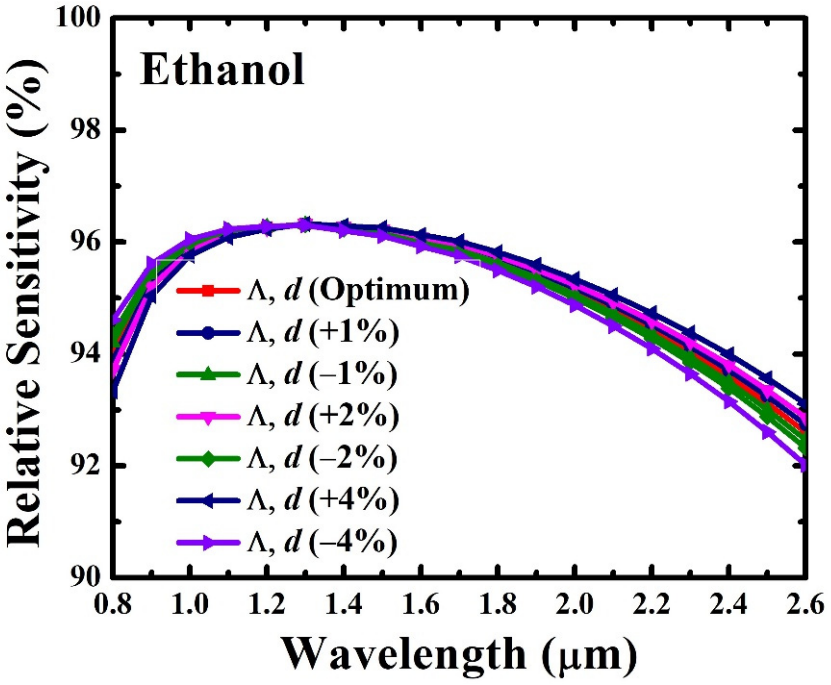

(**b**)

Figure 9. *Cont.*

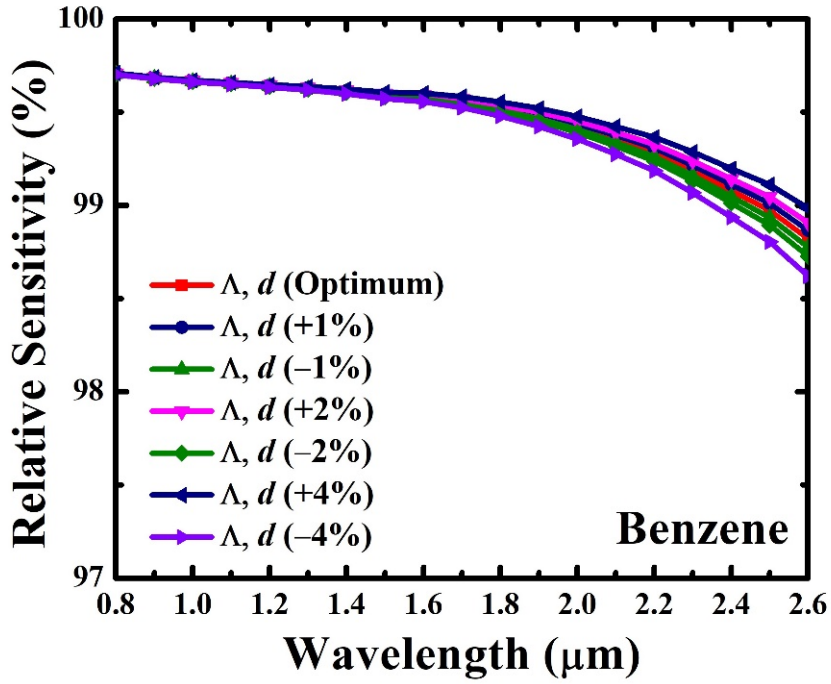

(**c**)

Figure 9. (**a**) Tolerance analysis of relative sensitivity for water in the variations of ±1%, ±2% and ±4%. (**b**) Tolerance analysis of relative sensitivity for ethanol in the variations of ±1%, ±2% and ±4%. (**c**) Tolerance analysis of relative sensitivity for benzene in the variations of ±1%, ±2% and ±4%.

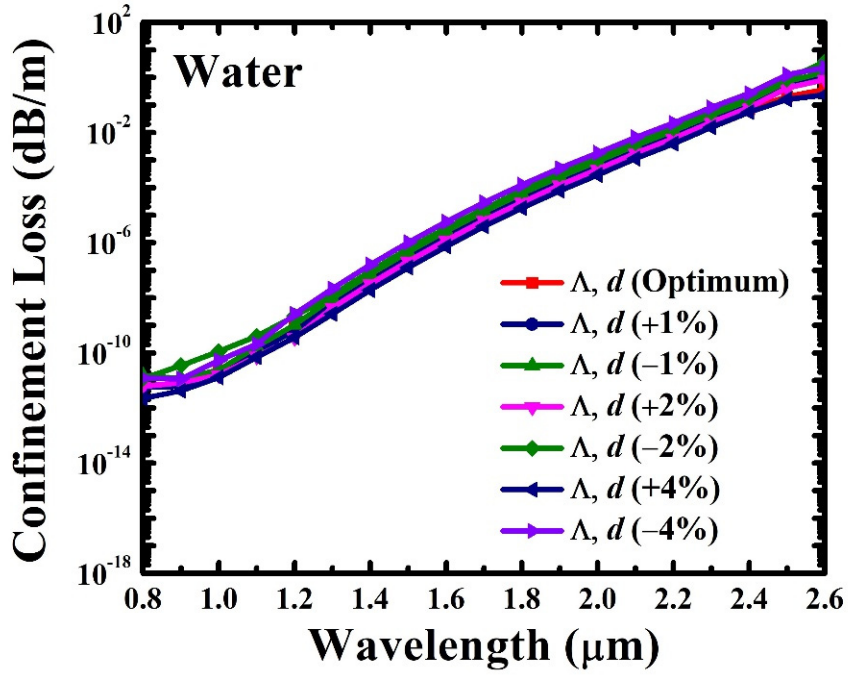

(**a**)

Figure 10. *Cont.*

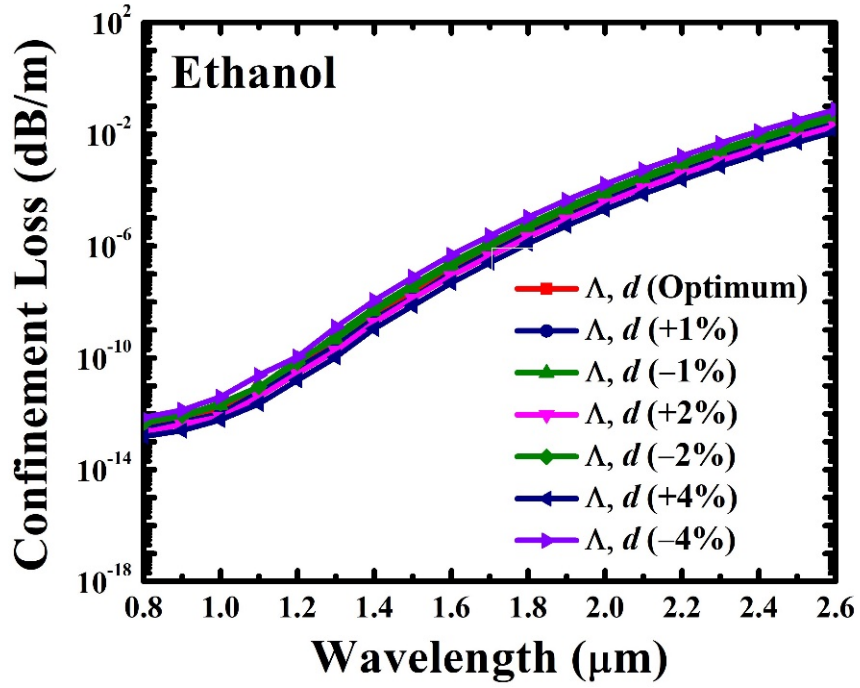

(**b**)

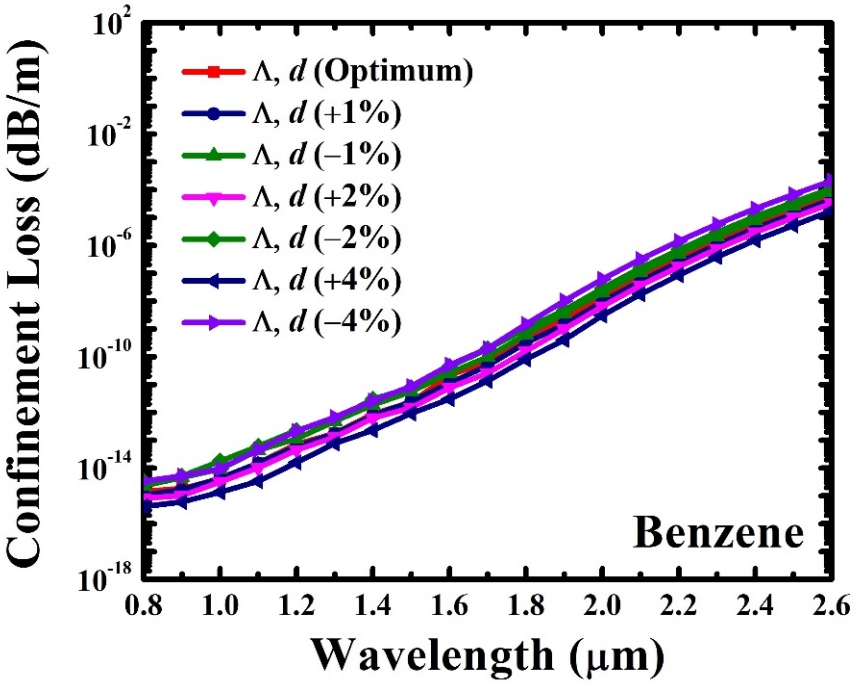

(**c**)

Figure 10. (**a**) Tolerance analysis of confinement loss for water in the variations of ±1%, ±2% and ±4%. (**b**) Tolerance analysis of confinement loss for ethanol in the variations of ±1%, ±2% and ±4%. (**c**) Tolerance analysis of confinement loss for benzene in the variations of ±1%, ±2% and ±4%.

Lastly, a comparison between prior PCF chemical sensors and the proposed PCF design is presented in Table 2. It can be observed from the table that the proposed PCF has a comparatively simple layout of a single core hole with two cladding rings, in contrast to the prior PCFs with additional cladding rings and intricate core designs. With regard to the design, the proposed PCF demonstrates the highest relative sensitivity and low

confinement loss, with all the chemical analytes. Therefore, the novelty of the proposed PCF is the simplicity of design, which aids in the ease of fabrication and leads to better numerically analyzed results.

Table 2. Comparison of structure and performance among prior PCFs and proposed PCF at λ = 1.3 µm.

	No. of Rings	Structure		Relative Sensitivity (%)	Confinement Loss (dB/m)
		Core	Cladding		
Ref. [9]	3	6 core holes	Circular holes in circle	26.23 (E)	~10^{-8} (E)
Ref. [10]	4	1 core hole	Circular holes in hexagon	41.37 (W)	~10^{-10} (W)
Ref. [11]	4	9 core holes	Circular holes in hexagon	44.45 (W)	~10^{-4} (W)
Ref. [12]	4	4 core holes	Circular holes in hexagon	49.13 (W)	~10^{-5} (W)
				48.19 (W)	
Ref. [13]	3	7 core holes	Circular holes in hexagon	53.22 (E)	-
				55.56 (B)	
				52.07 (W)	~10^{-13} (W)
Ref. [14]	5	9 core holes	Circular holes in octagon	56.75 (E)	~10^{-13} (E)
				58.86 (B)	~10^{-13} (B)
				62.60 (W)	~10^{-7} (W)
Ref. [15]	3	3 core holes	Circular holes in hexagon	65.34 (E)	~10^{-8} (E)
				74.50 (B)	~10^{-11} (B)
				90.14 (W)	~10^{-10} (W)
Ref. [16]	5	1 core hole	Circular holes in hexagon	93.85 (E)	~10^{-10} (E)
				98.11 (B)	~10^{-10} (B)
				94.47 (W)	~10^{-10} (W)
Proposed PCF	2	1 core hole	Circular holes in hexagon	96.32 (E)	~10^{-10} (E)
				99.63 (B)	~10^{-10} (B)

where W refers to water, E refers to ethanol and B refers to benzene.

5. Conclusions

The proposal of a simple PCF sensor for hazardous chemical detection has been introduced, which is composed of a single hexagonal hole for the core and 18 imposed cladding air holes, positioned in a hexagon-shaped lattice. Operating at the lower wavelengths of 0.8–2.6 µm, the designed chemical sensor with water, ethanol and benzene has been numerically analyzed with the aid of a FV-FEM simulation method on COMSOL Multiphysics to investigate its optical properties: effective refractive index, relative sensitivity, power fraction, confinement loss and chromatic dispersion. The optimum results have been obtained at a 1.3 µm operating wavelength, with high relative sensitivities of 94.47%, 96.32% and 99.63% for water, ethanol and benzene, respectively, and confinement losses of 7.31 × 10^{-9} dB/m, 3.70 × 10^{-10} dB/m and 1.76 × 10^{-13} dB/m for water, ethanol and benzene, respectively. The investigated results are noteworthy as they indicate the practicability of the proposed PCF for sensing applications in the medical sector, chemical industry, security and defense by sensing unknown analytes, as well as in optical communication through the desirable results of chromatic dispersion. Furthermore, this research shall potentially proceed to fabrication and experimental testing as future work.

Author Contributions: Conceptualization, A.M.M. and F.B.; methodology, A.M.M. and F.B.; software, A.M.M., S.K. and F.B.; validation, W.-R.W. and F.B.; formal analysis, A.M.M. and F.B.; investigation, A.M.M. and F.B.; resources, F.B.; data curation, A.M.M. and F.B.; writing—original draft preparation, A.M.M.; writing—review and editing, W.-R.W. and F.B.; visualization, F.B.; supervision, F.B.; project administration, F.B.; funding acquisition, F.B. and N.S. All authors have read and agreed to the published version of the manuscript.

Funding: This research was funded by UNIVERSITI BRUNEI DARUSSALAM, grant number UBD/RSCH/1.3/FICBF(b)/2019/008.

Institutional Review Board Statement: Not applicable.

Informed Consent Statement: Not applicable.

Data Availability Statement: Not applicable.

Conflicts of Interest: The authors declare no conflict of interest.

References

1. Habib, A.; Anower, S.; Haque, I. Highly Sensitive Hollow Core Spiral Fiber for Chemical Spectroscopic Applications. *Sens. Int.* **2020**, *1*, 100011. [CrossRef]
2. Abbott, D.; Zhang, X.C. Scanning the Issue: T-Ray Imaging, Sensing, and Retection. *Proc. IEEE* **2007**, *95*, 1509–1513. [CrossRef]
3. Habib, M.A.; Reza, M.S.; Abdulrazak, L.F.; Anower, M.S. Extremely High Birefringent and Low Loss Microstructure Optical Waveguide: Design and Analysis. *Opt. Commun.* **2019**, *446*, 93–99. [CrossRef]
4. Chang, Y.H.; Jhu, Y.Y.; Wu, C.J. Temperature Dependence of Defect Mode in a Defective Photonic Crystal. *Opt. Commun.* **2012**, *285*, 1501–1504. [CrossRef]
5. Bock, W.J.; Jiahua, C.; Eftimov, T.; Urbanczyk, W. A Photonic Crystal Fiber Sensor for Pressure Measurements. *Conf. Rec.-IEEE Instrum. Meas. Technol. Conf.* **2005**, *2*, 1177–1181. [CrossRef]
6. Chengkuo, L.; Thillaigovindan, J. Optical Nanomechanical Sensor Using a Silicon Photonic Crystal Cantilever Embedded with a Nanocavity Resonator. *Appl. Opt.* **2009**, *48*, 1797–1803. [CrossRef]
7. Morshed, M.; Imran Hassan, M.; Roy, T.K.; Uddin, M.S.; Abdur Razzak, S.M. Microstructure Core Photonic Crystal Fiber for Gas Sensing Applications. *Appl. Opt.* **2015**, *54*, 8637. [CrossRef]
8. Ademgil, H.; Haxha, S. PCF Based Sensor with High Sensitivity, High Birefringence and Low Confinement Losses for Liquid Analyte Sensing Applications. *Sensors* **2015**, *15*, 31833–31842. [CrossRef]
9. Asaduzzaman, S.; Ahmed, K. Microarray-Core Based Circular Photonic Crystal Fiber for High Chemical Sensing Capacity with Low Confinement Loss. *Opt. Appl.* **2017**, *47*, 41–49. [CrossRef]
10. Arif, M.F.H.; Hossain, M.M.; Islam, N.; Khaled, S.M. A Nonlinear Photonic Crystal Fiber for Liquid Sensing Application with High Birefringence and Low Confinement Loss. *Sens. Bio-Sens. Res.* **2019**, *22*, 100252. [CrossRef]
11. Bin Murshed Leon, M.J.; Abedin, S.; Kabir, M.A. A Photonic Crystal Fiber for Liquid Sensing Application with High Sensitivity, Birefringence and Low Confinement Loss. *Sens. Int.* **2021**, *2*, 100061. [CrossRef]
12. Leon, M.J.B.M.; Kabir, M.A. Design of a Liquid Sensing Photonic Crystal Fiber with High Sensitivity, Bireferingence & Low Confinement Loss. Sens. *Bio-Sens. Res.* **2020**, *28*, 100335. [CrossRef]
13. Islam, S.; Kumar, B.; Ahmed, K. Liquid-Infiltrated Photonic Crystal Fiber for Sensing Purpose: Design and Analysis. *Alexandria Eng. J.* **2018**, *57*, 1459–1466. [CrossRef]
14. Ahmed, K.; Morshed, M.; Asaduzzaman, S.; Arif, M.F.H. Optimization and Enhancement of Liquid Analyte Sensing Performance Based on Square-Cored Octagonal Photonic Crystal Fiber. *Optik* **2017**, *131*, 687–696. [CrossRef]
15. Maidi, A.M.; Yakasai, I.; Abas, P.E.; Nauman, M.M.; Apong, R.A.; Kaijage, S.; Begum, F. Design and Simulation of Photonic Crystal Fiber for Liquid Sensing. *Photonics* **2021**, *8*, 16. [CrossRef]
16. Eid, M.M.A.; Habib, M.A.; Anower, M.S.; Rashed, A.N.Z. Highly Sensitive Nonlinear Photonic Crystal Fiber Based Sensor for Chemical Sensing Applications. *Microsyst. Technol.* **2020**, *27*, 1007–1014. [CrossRef]
17. Buczynski, R. Photonic Crystal Fibers. *Acta Phys. Pol. Ser. A* **2004**, *106*, 141–167. [CrossRef]
18. Wang, P.; Farrell, G.; Semenova, Y.; Rajan, G. Influence of Fiber Manufacturing Tolerances on the Spectral Response of a Bend Loss Based All-Fiber Edge Filter. *Appl. Opt.* **2008**, *47*, 2921. [CrossRef]
19. Amouzad Mahdiraji, G.; Chow, D.M.; Sandoghchi, S.R.; Amirkhan, F.; Dermosesian, E.; Yeo, K.S.; Kakaei, Z.; Ghomeishi, M.; Poh, S.Y.; Yu Gang, S.; et al. Challenges and Solutions in Fabrication of Silica-Based Photonic Crystal Fibers: An Experimental Study. *Fiber Integr. Opt.* **2014**, *33*, 85–104. [CrossRef]
20. Lee, H.W.; Schmidt, M.A.; Uebel, P.; Tyagi, H.; Joly, N.Y.; Scharrer, M.; Russell, P.S.J. Optofluidic Refractive-Index Sensor in Step-Index Fiber with Parallel Hollow Micro-Channel. *Opt. Express* **2011**, *19*, 8200. [CrossRef] [PubMed]
21. El Hamzaoui, H.; Ouerdane, Y.; Bigot, L.; Bouwmans, G.; Capoen, B.; Boukenter, A.; Girard, S.; Bouazaoui, M. Sol-Gel Derived Ionic Copper-Doped Microstructured Optical Fiber: A Potential Selective Ultraviolet Radiation Dosimeter. *Opt. Express* **2012**, *20*, 29751. [CrossRef] [PubMed]
22. Kim, J.-C.; Kim, H.-K.; Paek, U.-C.; Lee, B.-H.; Eom, J.-B. The Fabrication of a Photonic Crystal Fiber and Measurement of Its Properties. *J. Opt. Soc. Korea* **2003**, *7*, 79–83. [CrossRef]
23. Zhang, P.; Zhang, J.; Yang, P.; Dai, S.; Wang, X.; Zhang, W. Fabrication of Chalcogenide Glass Photonic Crystal Fibers with Mechanical Drilling. *Opt. Fiber Technol.* **2015**, *26*, 176–179. [CrossRef]
24. Bertoncini, A.; Liberale, C. 3D Printed Waveguides Based on Photonic Crystal Fiber Designs for Complex Fiber-End Photonic Devices. *Optica* **2020**, *7*, 1487. [CrossRef]
25. Kiang, K.M.; Frampton, K.; Monro, T.M.; Moore, R.; Tucknott, J.; Hewak, D.W.; Richardson, D.J.; Rutt, H.N. Extruded Singlemode Non-Silica Glass Holey Optical Fibres. *Electron. Lett.* **2002**, *38*, 546–547. [CrossRef]
26. Huang, Y.; Xu, Y.; Yariv, A. Fabrication of Functional Microstructured Optical Fibers through a Selective-Filling Technique. *Appl. Phys. Lett.* **2004**, *85*, 5182–5184. [CrossRef]

27. Xiao, L.; Jin, W.; Demokan, M.S.; Ho, H.L.; Hoo, Y.L.; Zhao, C. Fabrication of Selective Injection Microstructured Optical Fibers with a Conventional Fusion Splicer. *Opt. Express* **2005**, *13*, 9014. [CrossRef]
28. Cordeiro, C.M.B.; dos Santos, E.M.; Brito Cruz, C.H.; de Matos, C.J.; Ferreiira, D.S. Lateral Access to the Holes of Photonic Crystal Fibers–Selective Filling and Sensing Applications. *Opt. Express* **2006**, *14*, 8403. [CrossRef]
29. Wang, Y.; Liu, S.; Tan, X.; Jin, W. Selective-Fluid-Filling Technique of Microstructured Optical Fibers. *J. Light. Technol.* **2010**, *28*, 3193–3196. [CrossRef]
30. Wang, F.; Yuan, W.; Hansen, O.; Bang, O. Selective Filling of Photonic Crystal Fibers Using Focused Ion Beam Milled Microchannels. *Opt. Express* **2011**, *19*, 17585. [CrossRef]
31. Arif, M.F.H.; Asaduzzaman, S.; Ahmed, K.; Morshed, M. High Sensitive PCF Based Chemical Sensor for Ethanol Detection. In Proceedings of the 2016 5th International Conference on Informatics, Electronics and Vision (ICIEV), Dhaka, Bangladesh, 13–14 May 2016; pp. 6–9. [CrossRef]
32. Malitson, I.H. Interspecimen Comparison of the Refractive Index of Fused Silica*,†. *J. Opt. Soc. Am.* **1965**, *55*, 1205. [CrossRef]
33. Hale, G.M.; Querry, M.R. Bladder Cancers Respond to EGFR Inhibitors. *Cancer Discov.* **2014**, *4*, 980–981. [CrossRef]
34. Moutzouris, K.; Papamichael, M.; Betsis, S.C.; Stavrakas, I.; Hloupis, G.; Triantis, D. Refractive, Dispersive and Thermo-Optic Properties of Twelve Organic Solvents in the Visible and near-Infrared. *Appl. Phys. B Lasers Opt.* **2014**, *116*, 617–622. [CrossRef]
35. Akowuah, E.K.; Gorman, T.; Ademgil, H.; Haxha, S.; Robinson, G.K.; Oliver, J.V. Numerical Analysis of a Photonic Crystal Fiber for Biosensing Applications. *IEEE J. Quantum Electron.* **2012**, *48*, 1403–1410. [CrossRef]
36. Yakasai, I.K.; Abas, P.E.; Ali, S.; Begum, F. Modelling and Simulation of a Porous Core Photonic Crystal Fibre for Terahertz Wave Propagation. *Opt. Quantum Electron.* **2019**, *51*, 1–16. [CrossRef]
37. Yakasai, I.; Abas, P.E.; Kaijage, S.F.; Caesarendra, W.; Begum, F. Proposal for a Quad-Elliptical Photonic Crystal Fiber for Terahertz Wave Guidance and Sensing Chemical Warfare Liquids. *Photonics* **2019**, *6*, 78. [CrossRef]
38. Begum, F.; Abas, P.E. Near Infrared Supercontinuum Generation in Silica Based Photonic Crystal Fiber. *Prog. Electromagn. Res. C* **2019**, *89*, 149–159. [CrossRef]
39. Begum, F.; Namihira, Y.; Kinjo, T.; Kaijage, S. Supercontinuum Generation in Photonic Crystal Fibres at 1.06, 1.31, and 1.55m Wavelengths. *Electron. Lett.* **2010**, *46*, 1518–1520. [CrossRef]
40. Begum, F.; Namihira, Y.; Razzak, S.M.A.; Kaijage, S.F.; Hai, N.H.; Miyagi, K.; Higa, H.; Zou, N. Flattened Chromatic Dispersion in Square Photonic Crystal Fibers with Low Confinement Losses. *Opt. Rev.* **2009**, *16*, 54–58. [CrossRef]